Molecular Motions in Polymer Films near the Glass Transition: a Single Molecule Study of Rotational Dynamics

Laura A. Deschenes and David A. Vanden Bout*

Department of Chemistry and Biochemistry, Center for Nano and Molecular Materials Science and Technology, and Texas Materials Institute, University of Texas, Austin, Texas 78712-1167

Received: June 13, 2001; In Final Form: September 11, 2001

Single molecule spectroscopy was used to measure the rotations of fluorescent probe molecules in thin films of poly(methyl acrylate) and poly(*n*-butyl methacrylate) just above their glass-transition temperatures. By collecting the polarized fluorescence from isolated probe molecules, the rotational diffusion of single molecules was followed in real time. The autocorrelation of these transients yields a nonexponential decay from which the rotational correlation time can be calculated. Molecules reveal a broad distribution of correlation times, which showed a clear dependence on the length of observation. At short times, the spatially heterogeneous nature of these films was reflected in their wide range of correlation times. At longer times, environmental exchanges caused the correlation times to converge on a limiting bulk value. The dynamics were characterized by three time scales: a rotational correlation time (τ_c), an environmental exchange time (τ_{ex}), and the time scale upon which the distribution of time-averaged single-molecule correlation times converged to the ensemble-averaged limit (τ_{bulk}). Both τ_{ex} and τ_{bulk} were much longer than τ_c, with the ensemble average τ_{ex} being approximately 20 times longer than the average τ_c and τ_{bulk} roughly 125 times τ_c. All three time scales were found to have the same relatively weak temperature dependence when measured at temperatures 5, 10, and 15 K above the glass transition.

Introduction

Amorphous solids are ubiquitous in both nature and technology; they are found in places ranging from volcanic rocks to the latest high-tech athletic shoes. Materials undergo significant changes as they are cooled from the liquid state to become an amorphous solid. Viscosity, for instance, increases by 13 orders of magnitude between the melting point and the glass transition,[1] but the disordered molecular structure of a liquid is retained throughout this cooling process and is ultimately "locked in" by the dynamic arrest that occurs with the onset of the glass transition. Despite the retention of normal liquid structure all the way from the melting temperature to the glass transition, the dynamic properties change dramatically as the system is cooled. Most notably, the many relaxation processes that appear as an exponential decay in normal liquids may become highly nonexponential near the glass transition. One common example is rotational reorientation, which follows a simple Brownian diffusional mechanism in normal liquids but is seen to deviate significantly near T_g. Although glass-forming materials have received much attention, both experimental and theoretical, uncertainties remain as to the nature and inherent time scales of molecular motions near the glass transition.

The problem of spatial and dynamic heterogeneity near the glass transition has prompted a great deal of research over the past decade.[2−13] While there remain some questions as to the extent and applicability of heterogeneity,[14,15] a large body of evidence has been built up for the existence and importance of domains of spatially heterogeneous dynamics in glass-forming materials ranging from simple small molecule liquids such as toluene,[16] glycerol,[17] and *ortho*-terphenyl[18−21] to complex high-molecular-weight polymers.[10,22−24] Because these materials still follow the laws of equilibrium statistical mechanics, ergodicity requires that the dynamics in these heterogeneous regions evolve in time until a single molecule samples all possible environments, at which point the time-averaged behavior becomes the same as the number-averaged behavior of an ensemble of molecules. This time required for the exchange of environments has been measured by a number of experimental techniques producing a wide variety of results. Early dynamic hole-burning experiments done with NMR[22,23,25,26] selected a subset of slowly relaxing environments and probed the time that it took for this subensemble to reproduce the bulk equilibrium dynamics. These studies, 10−20 K above T_g, found that the exchange time (how long it took to achieve bulklike behavior) was comparable to the relaxation time of the slow subset probed. Further dynamic hole-burning studies, this time utilizing an optical photobleaching technique, again measured the amount of time that it took for a slowly reorienting subset to become bulklike.[18,21,24] These experiments were performed much closer to T_g and found that for $T_g + 4$ K the exchange time was 10 times slower than the relaxation time but at $T_g + 1$ K the exchange time had become 10 000 times slower than the relaxation time. These optical and NMR results can be reconciled by assuming a strong temperature dependence for the exchange time, but other studies of dielectric properties using either hole-burning[17] or high-spatial-resolution microscopy [10,27] have found the exchange time to be either comparable to,[10] roughly twice as long as,[27] or much longer than[17] the relaxation time just above the glass transition. Clearly the question of exchange between heterogeneous environments near the glass transition remains a contentious issue, with the only real consensus being that it happens in many different types of glass-forming materials.

* To whom correspondence should be addressed. E-mail: davandenbout@mail.utexas.edu.

10.1021/jp012238v CCC: $20.00
Published on Web 11/02/2001

The development of single-molecule spectroscopy (SMS) as a probe for microscopic properties has opened a broad vista on molecular motions previously accessible only through simulation. Previous works have looked at single-molecule rotations in detail,[28,29] making real-time observation of rotational diffusion and the transitions of molecules between regions of different dynamics.[13] Single molecule spectroscopy is an advance in fluorescence spectroscopy that permits complex systems to be studied one molecule at a time. The key to SMS is in isolating a single fluorescent probe molecule, decreasing the background fluorescence from the sample, and increasing the single-molecule fluorescence to provide a reasonable signal-to-noise ratio. The great strength of SMS is its ability to apply standard fluorescence spectroscopy techniques to probe the chemical and physical properties of a molecule-sized environment within the sample.[13,28−38] By looking at molecules in different parts of the sample, variations in the local environment can be probed. Polarization-resolved SMS provides even more detail, as the dipolar nature of fluorescence excitation and emission can be exploited to determine the orientation of the molecule in the plane of the sample. This angle can be followed in time to extract information about the rotational properties of the microenvironment inhabited by the probe molecule.[13,29]

Using single-molecule spectroscopy, we are able to directly measure the rotational correlation times and the evolution of individual molecule-sized environments within a glass-forming polymer near the glass transition. We find that molecules retain a particular set of dynamics for a long period of time (10−25 times the average correlation time) before changing in a single dramatic step to a new set of dynamics. After a number of such switches, the molecule has sampled enough environments for its time-averaged dynamics to approach the ensemble average behavior. We find that at all of the temperatures tested it takes roughly 125 correlation times for the molecule to approach the limiting ensemble-like behavior. In addition, our single-molecule results allow us to measure how long the molecule retains a given set of dynamics, further elucidating the mechanism by which the spatially heterogeneous domains change dynamics with time.

Experimental Section

All single-molecule experiments were performed using a home-built sample-scanning inverted microscope. The second harmonic of a Nd:YAG laser (Crystalasers) was passed through a length of optical fiber, which serves as a spatial filter, and used as the excitation source. The sample temperature was held constant in a cryostat (Oxford Microstat N) mounted atop a closed loop $x-y$ piezo scanning stage (Queensgate). The excitation light was focused to a nearly diffraction-limited 600 nm spot using a super long working distance objective (Nikon 40x, 0.6 NA) corrected for the glass cryostat window. Excitation powers were typically between 0.5 μW (for imaging) and 0.02 μW (for transients). Fluorescence was collected through the same objective and passed through a series of dichroic and long-pass filters to remove excitation light. The fluorescence was then split into two orthogonal polarizations using a polarizing beam-splitting cube and imaged on the active area of two single-photon-counting avalanche photodiodes (EG&G). The small active area of the detectors served to limit the focal volume of light detected, although it was not strictly confocal. Data collection was correlated with sample scanning using a home-made Labview (National Instruments) program.

Samples were prepared from 2.5 wt % solutions in toluene of poly(methyl acrylate) (PMA, purchased from Aldrich, used as received) with $T_g = 281$ K and poly(*n*-butyl methacrylate) (P*n*BMA, purchased from Polysciences, used as received) with $T_g = 285$ K. Glass-transition temperatures were measured by differential scanning calorimetry. These solutions were doped with rhodamine 6G (R6G) in low (1−10 nM) concentrations. Rhodamine 6G was chosen for these experiments because of its high (near unit) fluorescence quantum yield and its low rate of intersystem crossing. The polymer solutions were then spin-cast on glass cover slips to make approximately 250 nm thick polymer films with spatially isolated probes. Films were held under vacuum for 2−24 h to ensure that all of the solvent had evaporated.

The measured transients consist of the anticorrelated fluorescence signals from the two orthogonal detectors, collected for as long as the molecule remains fluorescent. Because the molecules are rotating freely, the two signals vary smoothly and their anticorrelation arises as the emission dipole rotates from being aligned parallel with one detected polarization to being aligned parallel with the other. When the dipole is aligned parallel to one detected polarization, all the emitted photons are collected by that detector, giving a maximum in that channel and no signal above the dark counts inherent to the detector itself in the other. Because rotational diffusion is isotropic in three dimensions, both signals show correlated overall intensity variations due to the rotation of the probe molecule out of the plane of the sample, effectively reducing the overlap between the transition dipole and the exciting field and resulting in reduced emission rates.

From the orthogonal signals $I_S(t)$ and $I_P(t)$, defined with respect to the beam-splitting cube polarizations, the in-plane first quadrant angle of the molecule can be calculated according to

$$\theta(t) = \arctan\left(\sqrt{\frac{I_S(t)}{I_P(t)}}\right) \tag{1}$$

To ensure that the anticorrelated fluorescence signals observed were the result of real molecular rotation, the fluorescence signal was modulated by a rotating half wave plate, which switched the two linearly polarized signals between the two detectors in a sine-squared pattern with a frequency determined by the rotation rate but 90° out of phase. By fitting the phase of both signals with these constraints, the in-plane half angle of the emission dipole can be directly calculated. Because these measurements showed the same behavior as the quarter angle calculated from the two fluorescence signals, it was determined that the quarter angle measurement was sufficient to describe rotational dynamics. The quarter angle measurement has the significant advantage of permitting longer dwell times and correspondingly lower excitation powers, thereby effectively lengthening the photochemical survival time of each molecule.

Although the angle is the most intuitive measure of molecular rotation, most analyses are performed on a related quantity, the reduced linear dichroism, $A(t)$.

$$A(t) = \frac{I_S(t) - I_P(t)}{I_S(t) + I_P(t)} = \cos(2\theta) \tag{2}$$

$A(t)$ contains the same information as $\theta(t)$ but has several advantages in that the result ranges from −1 to 1, making it easy to calculate correlation functions and dividing by the total intensity eliminates artifacts due to laser fluctuation, spectral diffusion,[34] triplet blinking,[39] translational diffusion, or out-of-plane rotation.

When the molecule rotates fully out of plane, the signal on both detectors falls to a minimum that is determined by the inherent dark signal from the detectors (39 and 51 counts/s). This small constant background is subtracted from each signal, and the signals are also scaled with a small correction factor that accounts for differing detection efficiencies for the two polarizations.

The dynamics can be quantified by taking the autocorrelation, $C(t)$, of the dichroism signal $A(t)$. $C(t)$ is calculated using the standard method for discrete data points in finite time series. Confidence limits are calculated on the autocorrelations such that any points between the limits are consistent with zero.[40]

$$C(t) = \frac{\sum_{t'=0}^{T} A(t')A(t'+t)}{\sum_{t'=0}^{T} A(t')A(t')} \tag{3}$$

where T is the total number of points. $C(t)$ shows a decay which fits well to the Kholrausch−Williams−Watts (KWW) "stretched exponential" function

$$C(t) = \exp[-t/\tau_{KWW}]^{\beta} \tag{4}$$

where τ_{KWW} is the decay constant and where β goes from 0 to 1 with $\beta = 1$ recreating the single exponential expected for purely Brownian rotational diffusion. Decreasing β indicates an increasing deviation from pure single time diffusional behavior due to the incorporation of new rotational time scales. The β and τ_{KWW} parameters can be combined into a single number, the single-molecule correlation time, which gives the weighted average time scale for rotation.

$$\tau_c = \int_0^{\infty} C(t)\,dt = \frac{\tau_{KWW}}{\beta}\Gamma\left(\frac{1}{\beta}\right) \tag{5}$$

After measuring many molecules in the same sample, a distribution of single-molecule correlation times can be compiled. By averaging over this distribution, the ensemble average correlation time $\langle\tau_c\rangle$ can be determined, where N is the total number of molecules studied.

$$\langle\tau_c\rangle = \frac{1}{N}\sum_{i=0}^{N-1}(\tau_c)_i \tag{6}$$

A weighted average in which the total number of photons emitted per molecule was used as a weighting factor gave an average correlation time indistinguishable from the per-molecule average as defined in eq 6.

Recent work by Fourkas[41] has examined the problem of out-of-plane rotation in detail and concludes that fluorescence detected using a high NA objective contains an isotropic polarization component that arises when the emission dipole rotates up out of the plane of the sample. In the current work, this would appear as an additional dynamic background that varies on the same time scale as the signal. The net effect of this dynamic background is to bias the calculated angles $\theta(t)$ to 45°, which compresses the scale of $A(t)$ so that it no longer reaches the extreme values.

The fluorescence collected with a 1.2 NA objective from a molecule oriented in the $x-y$ plane will yield twice the fluorescence of an equally excited molecule oriented fully out of the plane. When the NA is reduced to 0.6 (as in this study), the signal is reduced by a factor of 4 but the collection efficiency for out-of-plane fluorescence is reduced by a factor of 24, yielding a signal-to-background ratio of 12:1. It should be noted, however, that out-of-plane molecules are not excited efficiently and the slow rotation of molecules in the polymer films coupled with the short fluorescence lifetime ensures that no molecule is likely to be excited in plane and emit out of plane. As a result of inefficient excitation, the amount of fluorescence detected from an out-of-plane molecule, and thus the fluctuating background, will be even smaller than the predicted $^1/_{12}$ of the signal.

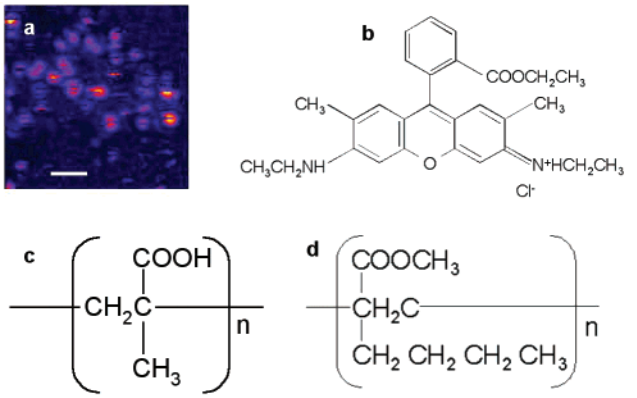

Figure 1. (a) A typical raster-scanned image of 10 nM rhodamine 6G in a 250 nm thick PMA film taken at $T_g + 10$ K. The scale bar indicates 1 μm. The chemical structures of (b) the fluorescent probe rhodamine 6G, (c) poly(methyl acrylate), and (d) poly(*n*-butyl methacrylate).

A simple Brownian random walk simulation was performed to test the effect of a fluctuating background on $C(t)$. In the simulation, transients were generated by allowing a dipole to make a random walk in space and looking at the in-plane projection of the dipole. The projections were used to calculate I_S and I_P. Differing amounts of a fluctuating background (generated in similar fashion) were added to these signals, resulting in a pair of transients that contained both correlated (background) and anticorrelated (signals) intensity fluctuations. These transients were then treated just like the experimentally determined I_S and I_P and used to calculate $A(t)$ and then $C(t)$. When fit to the KWW function, $C(t)$ showed no dependence upon the amount or time-scale of the added background until the background was over 3 times larger than the anticorrelated signals themselves, even when the background fluctuations were on the same time-scale as the in-plane rotational dynamics.

Results and Discussion

Figure 1 shows a typical raster scanned image of single molecules along with the chemical structures of the polymers and the dye probe. The concentration of the probe molecules was kept at such a low level that either one molecule was in the laser focus or no molecules were in the focus. The spots in the image then represent the fluorescence from individual molecules. The size of the spot reflects the size of the laser focus (because the molecules are much smaller than the laser). The spots can be verified to be single molecules by a number of factors. First, the number of molecules in any given image is similar to what one would expect from a 10 nM solution and a 250 nm film thickness. The number of molecules per unit area scaled linearly with the concentration of the dye solution used to make the films. The spots also show distinct polarization, which would be expected from individual transition dipoles. Last, and most importantly, the spots show both intermittent fluorescence blinking and single-step photobleaching kinetics. The blinking behavior is a single-molecule characteristic that

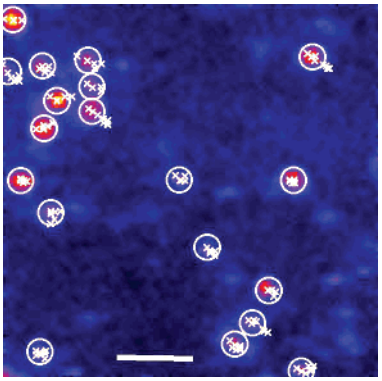

Figure 2. The total fluorescence intensity from a 10-μm image of R6G in PMA at $T_g + 10$ K. This is the first of a series of images taken over a 6-h period. The white circles correspond to the size of the laser spot (roughly 350 nm) centered on the initial position of each molecule, and the crosses depict the center of the molecule at successive half-hour intervals. The scale bar is 2 μm.

arises because of the molecule moving to its triplet excited state.[39] Because the triplet lifetime can be milliseconds long, the molecule is dark until it relaxes back to the ground state in which the fluorescence can be cycled. The single-step photobleaching is another important single-molecule characteristic that confirms the fact that the observed fluorescence comes from a single chromophore. When a chromophore is photochemically transformed into a different chemical, its quantum yield for fluorescence will drop dramatically and the absorption of the new species may no longer overlap with the excitation. When this happens, the molecule blinks off permanently. If all of the fluorescence detected in a given location is emitted from a single molecule, this photobleaching is seen as a single step rather than the decay that would be observed in an ensemble measurement. This photochemistry determines the total number of photons that can be collected from the molecule. While the cross section for these events is small, they will eventually occur due to the large number of times that the molecule is excited.

Single molecules were located spatially by imaging the sample, and transients were recorded by centering a located molecule in the laser focus. The fluorescence from the molecule in each polarization channel was recorded as a function of time with 0.02 μW excitation power and 1−2 s dwell times. In addition to providing temperature stability, the crysostat effectively removed atmospheric oxygen, extending the photochemical lifetime of the molecules by approximately a factor of 2.5, allowing for longer transients to be recorded. Typical transients lengths were 5000 s. Assuming a collection efficiency of 5%, this gives an average of 50 million photons emitted over the lifetime of the molecule. The removal of oxygen inhibited relaxation from the triplet state, as observed by longer off-time durations.[42] This effect is demonstrated in Figure 1, in which the dark lines across the molecules are due to triplet blinking. Although blinking results in significant signal fluctuations during imaging, it plays no role in the measured dynamics because transients are collected using a much lower excitation rate than are images, reducing the opportunities for intersystem crossing. In addition, because triplet blinking is so much faster than the 1−2 s dwell times, even with the long triplet lifetime, the molecule is never dark for a significant fraction of the measurement period.

To take long transients, the scanning stage must be stable for long periods of time and the molecules must not translationally diffuse out of the laser focus. The stability of the stage was assured by using a linearized closed-loop piezo stage. This

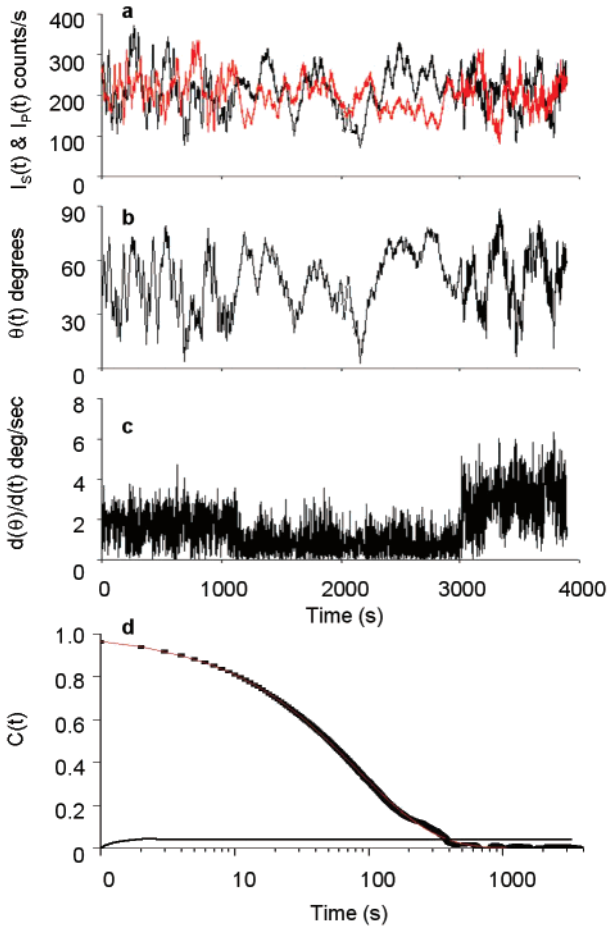

Figure 3. A typical single-molecule transient in PMA at $T_g + 10$ K, shown throughout the data analysis process. Panel a shows the raw signals from the two orthogonal detectors with the clear anticorrelation due to molecular rotation. In panel b, these signals have been combined to calculate the in-plane orientation of the emission dipole. Panel c shows the time derivative of this angle, accentuating the sudden changes between rotation rates. The autocorrelation of this transient is shown in panel d and fit to the KWW function with $\tau_{KWW} = 81$ s and $\beta_{KWW} = 0.741$, yielding $\tau_c = 97$ s. Confidence limits are calculated such that any points between the limits are consistent with zero.

stage has active capacitance measurement of position to remove the effect of piezo creep. This was verified by recording transients of a 100 nm fluorescent sphere (Polysciences) centered in the laser focus. The total intensity of the fluorescence did not vary over the course of 4 h. The lateral diffusion of the molecules was estimated by repeatedly imaging a single-molecule sample over the course of many hours. Figure 2 shows the first of a series of repeated images of the same area collected over a 6-h period. The white circle shows the approximate size of the laser spot (350 nm) centered on the initial position of each molecule, and the white crosses reflect the center position of the molecule in each successive scan (30 min apart). Even over this extended period, few molecules translate out of the laser focus, permitting extremely long transients to be recorded with a fixed microscope position. These images were collected using a 1.2 NA objective, resulting in a 350 nm laser spot. Because few molecules translate even that far, it becomes increasingly unlikely that molecules will diffuse out of the 600 nm spot formed by the 0.6 NA objective used for collecting transients.

A typical single-molecule transient is depicted in Figure 3, in which the parallel and perpendicular fluorescence signals exhibiting anticorrelation due to molecular rotation are shown

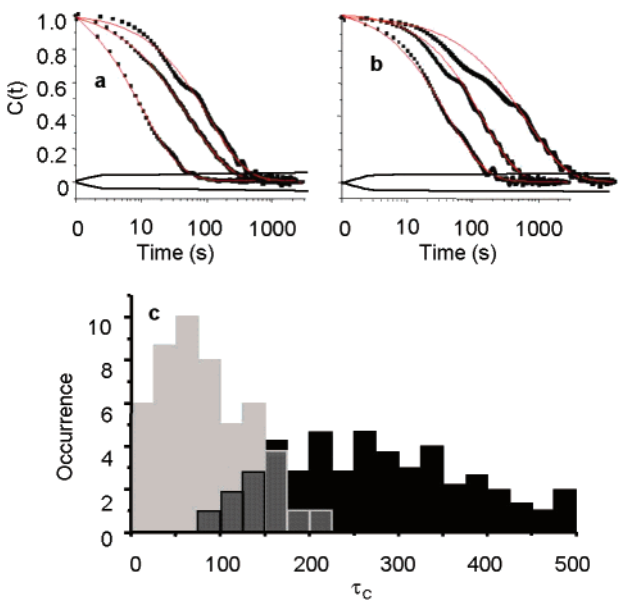

Figure 4. Representative correlation functions for PMA and P*n*BMA at the same temperature (291 K), illustrating the breadth of environments found in both polymers. Panel a shows three correlation functions in PMA at $T_g + 10$ K fit to the KWW function with $\tau_{KWW} = 15$ s and $\beta_{KWW} = 0.824$, $\tau_{KWW} = 107$ s and $\beta_{KWW} = 0.714$, and $\tau_{KWW} = 153$ s and $\beta_{KWW} = 0.802$. In panel b, correlation functions in P*n*BMA ($T_g + 6$ K) are shown with $\tau_{KWW} = 125$ s and $\beta_{KWW} = 0.839$, $\tau_{KWW} = 208$ s and $\beta_{KWW} = 0.776$, and $\tau_{KWW} = 371$ s and $\beta_{KWW} = 0.614$. Confidence limits on the correlation functions are calculated such that any points between the limits are consistent with zero. Histograms of the single-molecule correlation times measured in these polymers are shown in panel c with PMA in gray and P*n*BMA in black.

in panel a, and the resulting orientation of the transition dipole is shown in panel b. The abrupt changes in observed dynamics are demonstrated in panel c because it plots the time derivative of the orientation, and finally, the rotational autocorrelation function for this transient is depicted in panel d, along with its fit to the KWW equation, yielding $\tau_{KWW} = 81$ s, $\beta_{KWW} = 0.741$, and $\tau_c = 97$ s.

Individual molecules show remarkably different behavior from one another, and molecules in PMA and P*n*BMA show distinctly different qualitative behaviors at room temperature. The molecules in PMA ($T_g + 10$ K) rotate markedly faster than those in P*n*BMA ($T_g + 6$ K). This shows that the single-molecule motions are reflective of polymer properties and not caused by a photochemical effect solely dependent on the absolute temperature. Figure 4 shows several single-molecule correlation functions taken in both PMA (panel a) and P*n*BMA (panel b). In both polymers, molecules in different regions of the film showed different dynamics, a clear indication of spatial heterogeneity. Panel c shows the distribution of correlation times for both of these polymers at 291 K. PMA (in gray, at $T_g + 10$ K), which is farther from the glass transition, has shorter correlation times than does P*n*BMA (in black, at $T_g + 6$ K), which is closer to the glass transition. P*n*BMA shows a wider distribution of correlation times than does PMA. Because the magnitude and shape of the distribution of correlation times, τ_c, for single molecules vary with different materials and temperatures, the ensemble average correlation time, $\langle\tau_c\rangle$, becomes an important means of comparing dynamics in different systems.

To make sure that there were no photoinduced artifacts in the measured dynamics due to the continuous excitation of the probe molecule, experiments were performed at excitation powers that varied by a factor of 25. Dynamics measured with excitation powers of 5 μW and 0.02 μW had τ_{KWW} and β_{KWW} distributions that were indistinguishable. Furthermore, when these results are combined into an ensemble correlation function, they gave the same values for $\langle\tau_{KWW}\rangle$, $\langle\beta_{KWW}\rangle$, and $\langle\tau_c\rangle$. These results are summarized in Table 1.

TABLE 1: Ensemble Average KWW Parameters at 291 K Showing the Independence of Dynamics on Excitation Power and Film Thickness while Emphasizing the Difference between PMA and P*n*BMA

	$\langle\tau_{KWW}\rangle$ (s)	$\langle\beta_{KWW}\rangle$	$\langle\tau_c\rangle$ (s)
P*n*BMA, 250 nm, 0.02 μW	187	0.486	349
PMA, 250 nm, 0.02 μW	35	0.413	106
PMA, 250 nm, 0.5 μW	33	0.413	100
PMA, 1000 nm, 0.02 μW	42	0.451	103

Had any component of the dynamics been photodriven, the higher power transients would have shown shorter ensemble average correlation times,[34] but because no variation in the dynamics was seen with higher excitation rates, the measured dynamics were assumed to be inherent to the polymer and not photodriven.

As reported previously,[13] single-molecule correlation times in both polymers vary greatly within the same film, a clear indication that these materials are spatially heterogeneous. Examination of the transients gives hints as to the origin of these heterogeneities: some molecules move slowly, some move rapidly, and a great many of them switch from fast to slow or vice versa during the course of the transient. Figure 3 shows a transient that undergoes several distinct changes in dynamics throughout its photochemical lifetime. These switches are difficult to see in the raw data (Figure 3, panel a), but show up as distinct level changes in the time derivative of the angle (Figure 3, panel c). One possible explanation for this behavior is an interaction between the molecules and the glass substrate; when the molecule interacts strongly with the glass, it moves slowly, and when it interacts less strongly, it moves more rapidly. To test this effect, two experiments were performed. First, the fluorescence intensities of more concentrated dye-doped films cast on plain glass and on indium−tin oxide (ITO)-coated glass were measured. Because ITO is known to quench fluorescence,[43] a large population of dye molecules located at the surface would appear as a reduction of total fluorescence intensity. The fluorescence intensity from 250 nm thick films similar to those used in the SMS experiments was found to be identical on the ITO and glass surfaces indicating that few if any of the molecules were located near the surface. In addition, single-molecule dynamics were measured in thicker films. If the surface played a large role in the dynamics, a strong dependence on the film thickness would be expected. Individual transients and a reconstructed ensemble measured in 1000 nm thick films were identical to those in the 250 nm films used in this study (see Table 1). The thinner films were used for most of the work because they had a smaller background signal and provided higher signal-to-noise ratios for the transients.

Because the fast changes in dynamics are found to be independent of film thickness and are not due to interactions between the molecule and the surface, they must be related to a property of the polymer. Analysis of the single-molecule transients can give information about not only the dynamics of a particular microenvironment but also how long these dynamics persist before the environment changes again, a time we define as τ_{ex}, the exchange time, described at length in a previous publication.[13] One interpretation of these exchange times is that they are the result of a diffusional process with a time constant

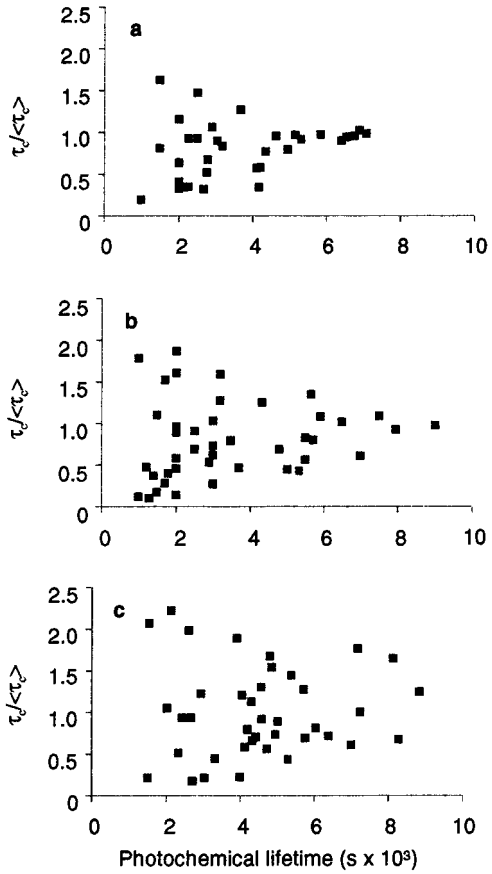

Figure 5. Single-molecule correlation times, τ_c, normalized by the ensemble average correlation time, $\langle\tau_c\rangle$, as a function of photochemical lifetime in PMA at (a) $T_g + 15$ K, (b) $T_g + 10$ K, and (c) $T_g + 5$ K.

much slower than that for normal rotational diffusion, but such a mechanism would give rise to an exponential distribution of exchange times with a well-defined temperature dependence, which is not the case for our measured exchange times. It has been conjectured that these switches may be related to a large-scale collective motion of the local polymer environment, because other experiments[12] and simulations[5,44] of glass-forming materials have shown sudden changes in translational dynamics due to cooperative motion of many particles.

Because of these long environmental exchange times, the measured dynamics of any given molecule depend not only on its local environment but also on how long it emits before irreversible photochemistry occurs. The molecules that live longest switch environments many times so that their time-averaged dynamics also reflect an ensemble-average of different environments. Shorter-lived molecules photobleach before they have sampled many different environments and therefore show greater variation in correlation times, as shown in Figure 5. At long photochemical survival times, the distribution of single-molecule correlation times, τ_c, converges to a limiting value that agrees with the ensemble average correlation time $\langle\tau_c\rangle$. Thus, the amount of time that it takes for the variation in single-molecule correlation times to vanish is a measure of the amount of time (τ_{bulk}) that it takes a single molecule to sample the entire distribution of dynamics or the time at which its correlation time converges to the ensemble average value.

The data in Figure 5 can be binned into 1000 s blocks, and the standard deviation of the population of each bin can be calculated. This result is plotted in Figure 6, which confirms that short transients have a broad distribution of correlation times resulting in a large standard deviation and as the transients

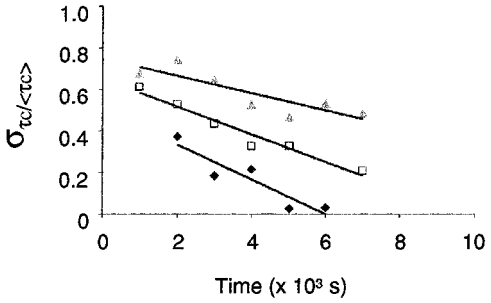

Figure 6. The standard deviation of the normalized single-molecule correlation times in PMA from Figure 5 taken in 1000 s blocks and plotted as a function of the photochemical lifetime of the molecule. Data are shown at $T_g + 15$ K (black diamonds), $T_g + 10$ K (unfilled squares), and $T_g + 5$ K (gray triangles). The lines are linear least-squares fits to the data, yielding values of τ_{bulk} of 5979, 9758, and 17 841 s, respectively.

become longer the distribution narrows and the standard deviation drops. The lower-temperature molecules start out with a broader distribution of τ_c and take longer to converge than do the ones farther from T_g. A linear least-squares regression was used to fit the data, and from these fits, the point at which the data cross the *x*-axis at zero standard deviation gives a measure of τ_{bulk}. These calculated values for τ_{bulk} range from 6000 $\pm$ 1700 s to 11 000 $\pm$ 1300 s to 18 000 $\pm$ 4900 s (error bars are calculated from the standard error in the fits) as the temperature is reduced from $T_g + 15$ K to $T_g + 10$ K to $T_g + 5$ K.

Previous studies of heterogeneous dynamics have looked at only two time scales: τ_c, the average correlation time, and τ_{bulk}, the time it takes for the heterogeneity to relax back to an isotropic bulk value. The current work looks at three times: τ_c, τ_{bulk}, and, in addition, τ_{ex}, the length of time the molecule retains a particular set of dynamics. While τ_c and τ_{bulk} are determined from the autocorrelation of rotational data, τ_{ex} is measured directly from the single-molecule transient and is identified by distinct changes in rotation rate. Although τ_{bulk} and τ_{ex} are necessarily related because the faster a molecule exchanges environments the faster it will sample the whole ensemble, τ_{ex} provides independent information on the distribution and lifetime of these environments inaccessible through the correlation function. The temperature dependence of these times and the changing shape of their distributions help to describe the way molecular rotations slow as the system approaches the glass transition. The temperature dependence of the ensemble average correlation time is shown in Figure 7a, in which the error bars are indicative of the standard deviation of the distribution, incorporating transients of all lengths. The correlation time shows a surprisingly modest temperature dependence. The temperature dependence measured for the correlation times is weaker than that reported by many bulk studies in this temperature range.[45,46] The α-relaxation time in PMA varies by more than 2 orders of magnitude from $T_g + 15$ K to $T_g +$ 5 K, while the τ_c measured by SMS decreases only by a factor of 3. To confirm that dynamics slow dramatically at the glass transition, several measurement attempts were made a few degrees below T_g. It was found that within a few degrees of T_g ($T_g - 3$ K) the dynamics are so slow that what little rotation occurs during the photochemical lifetime of the probe molecule is often obscured by the shot noise inherent to the measurement. However, on the basis of the apparent rate of angle change for the most mobile molecules, it can be estimated that the correlation time can be no shorter than 5000 s at this temperature.

τ_{ex} and τ_{bulk} show similarly weak temperature dependence, depicted in Figure 7, panel b (error bars are given by the

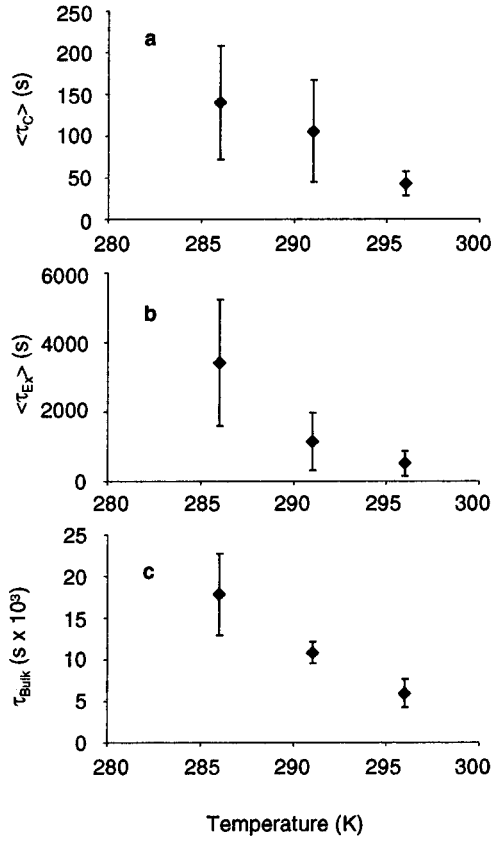

Figure 7. Ensemble average time scales as a function of temperature. Panel a shows ensemble average correlation times, $\langle\tau_c\rangle$. The error bars on all three plots are the ensemble standard deviation and in this case represent a maximum value because they are not corrected for the inherent spread due to different photochemical lifetimes (see Figure 5). Panel b shows average exchange times, $\langle\tau_{ex}\rangle$, as determined directly from $d(\theta)/d(t)$ (see Figure 4). Panel c is the averaging time, τ_{bulk}: the time required for a single molecule to sample enough different time scales for $\tau_c = \langle\tau_c\rangle$.

standard deviation of the distribution) and panel c. While the exchange time appears to increase at a slightly greater rate as the glass transition approaches, the broad distributions of both τ_c and τ_{ex} make it difficult to determine definitively. It can be seen from these plots that τ_c, τ_{ex}, and τ_{bulk} show basically the same temperature dependence. When the ratio of τ_{bulk} to τ_c is taken, it can be seen that at all three temperatures it takes roughly 125 correlation times for the environment to appear bulklike. Another measure of relative dynamics, the number of environmental exchanges required for a single molecule to achieve bulklike behavior, can be determined from the ratio of τ_{bulk} to τ_{ex}. This analysis indicates that it takes only a few (5−10) exchanges to sample the whole ensemble, and once again the broad distributions of exchange times ensure that any identifiable temperature dependence falls within the error bars. Because the distribution of dynamics broadens near T_g, the absolute change in dynamics per exchange must become larger for the same number of exchanges to sample the whole distribution.

Conclusions

We have found single-molecule spectroscopy to be a sensitive probe of heterogeneous rotational dynamics near the glass transition, capable of directly observing spatial heterogeneity in polymer systems at temperatures ranging from $T_g + 15$ K to $T_g - 3$ K, although the dynamic behavior is difficult to quantify at this lowest temperature because of extremely slow molecular motions. We have measured rotational dynamics in two different polymer systems and found that they both show distinct spatial heterogeneity characterized by discrete environmental changes. The measured dynamics are found to depend on both the proximity of the glass transition and the characteristics of the polymer, because it is found that PMA has significantly shorter correlation times at $T_g + 5$ K than does P*n*BMA at $T_g + 6$ K.

Rotational correlation times are found to depend strongly on the photochemical survival time of the fluorescent probe, indicating that molecules exchange environments on a time scale faster than the photochemical lifetime. These exchanges can be observed directly from the single-molecule transients, in which they appear as distinct level changes in the rotation rate of the molecule. Furthermore, the measured distributions of τ_c and τ_{ex} broaden as the temperature is reduced toward the glass transition. Because the heterogeneous microenvironments occupied by single molecules are not static, eventually the molecule will sample enough different environments that its time-averaged dynamics will reflect the ensemble-averaged behavior of the material. A measure of this time that it takes for a single molecule to reach ensemble-average behavior can be determined by extrapolating the photochemical lifetime of a single probe to a time at which the distribution of correlation times would narrow to a single value, reflective of the ensemble average correlation time. Characterization of the dynamics is found to incorporate three time scales: the rotational correlation time, environmental exchange time, and the time for a single molecule to give bulklike dynamics. Despite the changing distributions, all of the characteristic time scales have a similar but weak temperature dependence from $T_g + 15$ K to $T_g + 5$ K. This result is unexpected because past studies of the α-relaxation of these polymers have shown greater dependence on temperature in this range.[45,46] Because of the characteristic spatial heterogeneity in these materials, as well as the dependence of dynamics on photochemical lifetime, probe molecules at the same temperature show a broad distribution of correlation and exchange times. On average, it takes 10−25 correlation times before the molecules exchange environments, and between 5 and 10 exchanges for them to achieve an ergodic, ensemble average behavior.

The weak temperature dependence observed raises interesting questions about the ensemble of environments probed by SMS, because other studies that have measured the time required for a heterogeneous ensemble to give bulklike dynamics show a strong temperature dependence, ranging from τ_{bulk} comparable to τ_c[23] to τ_{bulk} many times larger than τ_c for lower temperatures.[24] Our results show that at all of the temperatures probed $\tau_{bulk} \approx 125\tau_c$, with little variation with temperature. These results emphasize the importance of heterogeneous domains in determining the measured dynamics of glass-forming materials, because it is not clear that the single-molecule experiments probe the same set of microdomains as do the traditional bulk probe relaxation experiments. Further studies will attempt to resolve this quandary by measuring the reorientational relaxation of bulk systems of rhodamine 6G in PMA to directly compare these single-molecule results with the α-relaxation of this polymer. In addition, experiments with different fluorescent probes in better-characterized polymer and supercooled liquid systems will help clarify what role, if any, specific dye−polymer interactions play in the observed heterogeneous dynamics.

Acknowledgment. D.A.V.B. is a Research Corporation Cottrell Scholar and a Camille and Henry Dreyfus Foundation New Faculty Awardee. This work is supported by grants from the Research Corporation.

References and Notes

(1) Fourkas, J. T., Kivelson, D., Mohanty, U., Nelson, K. A., Eds. *Supercooled Liquids: Advances and Novel Applications*; ACS Symposium Series 676; American Chemical Society: Washington, DC, 1997; p 352.

(2) Angell, C. A.; Ngai, K. L.; McKenna, G. B.; McMillan, P. F.; Martin, S. W. *J. App. Phys.* **2000**, *88*, 3113−3157.

(3) Chang, I.; Sillescu, H. *J. Phys. Chem. B* **1997**, *101*, 8794−8801.

(4) Böhmer, R.; Chambelin, R. V.; Diezemann, G.; Geil, B.; Heuer, A.; Hize, G.; Kuebler, S. C.; Richert, R.; Schiener, B.; Sillescu, H.; Speiss, H. W.; Tracht, U.; Wilhelm, M. *J. Non-Cryst. Solids* **1998**, *235*−*237*, 1−9.

(5) Bennemann, C.; Donati, C.; Baschnagel, J.; Glotzer, S. C. *Nature* **1999**, *399*, 246−249.

(6) Wang, C.-Y.; Ediger, M. D. *J. Phys. Chem. B* **1999**, *103*, 4177−4184.

(7) Sillescu, H. *J. Non-Cryst. Solids* **1999**, *243*, 81−108.

(8) Ediger, M. D. *Annu. Rev. Phys. Chem.* **2000**, *51*, 99−128.

(9) Ngai, K. L. *J. Non-Cryst. Solids* **2000**, *274*, 155−161.

(10) Russell, E. V.; Israeloff, N. E. *Nature* **2000**, *408*, 695−698.

(11) Wang, C.-Y.; Ediger, M. D. *J. Phys. Chem. B* **2000**, *104*, 1724−1728.

(12) Weeks, E. R.; Crocker, J. C.; Levitt, A. C.; Schofield, A.; Weitz, D. A. *Science* **2000**, *287*, 627−630.

(13) Deschenes, L. A.; Vanden Bout, D. A. *Science* **2001**, *292*, 255−258.

(14) Ngai, K. L. *J. Phys. Chem. B* **1999**, *103*, 10684−10694.

(15) Cugliandolo, L. F.; Iguain, J. L. *Phys. Rev. Lett.* **2000**, *85*, 3448−3451.

(16) Hinze, G. *Phys. Rev. E* **1998**, *57*, 2010−2018.

(17) Schiener, B.; Chamberlin, R. V.; Diezemann, G.; Bohmer, R. *J. Chem. Phys.* **1997**, *107*, 7746−7761.

(18) Cicerone, M. T.; Ediger, M. D. *J. Phys. Chem.* **1993**, *97*, 10489−10497.

(19) Böhmer, R.; Hinze, G.; Diezemann, G.; Geil, B.; Sillescu, H. *Europhys. Lett.* **1996**, *36*, 55−60.

(20) Cicerone, M. T.; Ediger, M. D. *J. Chem. Phys.* **1996**, *104*, 7210−7218.

(21) Wang, C.-Y.; Ediger, M. D. *J. Phys. Chem. B* **1999**, *103*, 4177.

(22) Heuer, A.; Wilhelm, M.; Zimmermann, H.; Speiss, H. W. *Phys. Rev. Lett.* **1995**, *75*, 2851−2854.

(23) Kuebler, S. C.; Heuer, A.; Spiess, H. W. *Phys. Rev. E* **1997**, *56*, 741−749.

(24) Wang, C.-Y.; Ediger, M. D. *J. Chem. Phys.* **2000**, *112*, 6933−6937.

(25) Schmidt-Rohr, K.; Speiss, H. W. *Phys. Rev. Lett.* **1991**, *66*, 3020−3023.

(26) Hinze, G.; Diezemann, G.; Sillescu, H. *Europhys. Lett.* **1998**, *44*, 565−570.

(27) Russell, E. V.; Israeloff, N. E.; Walther, L. E.; Gomariz, H. A. *Phys. Rev. Lett.* **1998**, *81*, 1461−1464.

(28) Ha, T.; Glass, J.; Enderle, T.; Chemla, D. S.; Weiss, S. *Phys. Rev. Lett.* **1998**, *80*, 2093−2096.

(29) Dickson, R. M.; Bartko, A. P. *J. Phys. Chem. B* **1999**, *103*, 3053−3056.

(30) Ambrose, W. P.; Moerner, W. E. *Nature* **1991**, *349*, 225−227.

(31) Moerner, W. E. *Science* **1994**, *266*, 46−53.

(32) Basche, T.; Kummer, S.; Braeuchle, C. *Nature* **1995**, *373*, 132−134.

(33) Schmidt, T.; Schuetz, G. J.; Baumgratner, W.; Gruber, H. J.; Schindler, H. *Proc. Nat. Acad. Sci. U.S.A.* **1996**, *93*, 2926−2929.

(34) Lu, H. P.; Xie, X. S. *Nature* **1997**, *385*, 143−146.

(35) Ha, T.; Laurence, T. A.; Chemla, D. S.; Weiss, S. *J. Phys. Chem. B* **1999**, *103*, 6839−6850.

(36) English, D. S.; Furube, A.; Barbara, P. F. *Chem. Phys. Lett.* **2000**, *324*, 15−19.

(37) Talley, C. E.; Dunn, R. C. *J. Phys. Chem.* **1999**, *103*, 10214−10221.

(38) Hou, Y.; Bardo, A. M.; Martinez, C.; Higgins, D. A. *J. Phys. Chem.* **2000**, *104*, 212−219.

(39) Veerman, J. A.; Garcia-Parajo, M. F.; Kuipers, L.; van Hulst, N. F. *Phys. Rev. Lett.* **1999**, *83*, 2155−2158.

(40) Box, G. E. P.; Jenkins, G. M. *Time Series Analysis Forecasting and Control*; Holden-Day: San Francisco, CA, 1976.

(41) Fourkas, J. T. *Opt. Lett.* **2000**, *26*, 211.

(42) Weston, K. D.; Carson, P. J.; DeAro, J. A.; Butatto, S. K. *Chem. Phys. Lett.* **1999**, *308*, 58.

(43) Lu, H. P.; Xie, X. S. *J. Phys. Chem. B* **1997**, *101*, 2753−2757.

(44) Kob, W.; Donati, C.; Plimpton, S. J.; Poole, P. H.; Glotzer, S. C. *Phys. Rev. Lett.* **1997**, *79*, 2827−2830.

(45) Sanchís, A.; Prolongo, M. G.; Masegosa, R. M.; Rubio, R. G. *Macromolecules* **1995**, *28*, 2693.

(46) Prolongo, M. G.; Salom, C.; Masegosa, R. M.; Moreno, S.; Rubino, R. G. *Polymer* **1997**, *38*, 5097−5105.